Bifunctional Application of Lithium Ferrites (Li_5FeO_4 and $LiFeO_2$) During Carbon Monoxide (CO) Oxidation and Chemisorption Processes. A Catalytic, Thermogravimetric and Theoretical Analysis

Hugo A. Lara-García,[1] Elizabeth Vera,[1] J. Arturo Mendoza-Nieto,[1] J. Francisco Gómez-García,[1] Yuhua Duan[2] and Heriberto Pfeiffer[1,*]

[1]*Laboratorio de Fisicoquímica y Reactividad de Superficies (LaFReS), Instituto de Investigaciones en Materiales, Universidad Nacional Autónoma de México, Circuito exterior s/n, Cd. Universitaria, Del. Coyoacán C.P. 04510, Ciudad de México, Mexico.*

[2]*National Energy Technology Laboratory, United States Department of Energy, 626 Cochrans Mill Road, Pittsburgh, Pennsylvania 15236, United States.*

**Corresponding author: Phone +52 (55) 5622 4627, fax +52 (55) 5616 1371 and E-mail pfeiffer@iim.unam.mx*

Abstract: The CO oxidation and subsequent CO_2 chemisorption processes were evaluated using two lithium ferrites, Li_5FeO_4 and $LiFeO_2$, as possible catalytic and captor materials. The analysis of the bifunctional process was dynamic and isothermally evaluated using catalytic and thermogravimetric techniques, while solid final products were characterized by X-ray diffraction (XRD), X-ray photoelectron spectroscopy (XPS) and temperature programmed desorption (TPD). These experiments were performed using a CO-O_2 mixture or only CO as gas flows. In addition, different *ab initio* thermodynamic calculations were performed to elucidate the theoretical viability of these processes. Thermogravimetric and catalytic results clearly showed that both lithium ferrites were able to perform the CO

oxidation and CO_2 chemical capture. The efficiency and reaction mechanism varied as a function of the lithium ferrite (Li_5FeO_4 or $LiFeO_2$), gas mixture and temperature. As it would be expected, Li_5FeO_4 sample presented better catalytic and chemisorption properties than $LiFeO_2$, regardless the gas mixture employed (CO or $CO+O_2$). Moreover, catalytic tests showed that the reaction process was produced even in the oxygen absence. In such a case, both lithium ferrites released the oxygen necessary for the oxidation process with a consequent iron reduction, as it was observed by XRD. Based on the obtained experimental and theoretical results, reaction mechanisms were proposed for each lithium ferrite into this bifunctional process. Finally, the best catalytic behavior was obtained with the Li_5FeO_4-CO-O_2 system, where high CO conversions (50-75 %) were observed between 500-650 °C and T > 800 °C. Also according to TGA results, this system at T > 700 °C presented the highest ability for capture the CO_2 previously formed during the CO oxidation process (~45 %).

Keywords: CO oxidation; CO_2 chemisorption; *ab initio* thermodynamics; Lithium ferrites; Thermogravimetric analysis

Introduction

The dependence in our current energy system, based in fossil fuels, has produced serious environmental problems, where one of the principal issues is the increment of the global surface temperature caused by the high concentration of the greenhouse gases in the atmosphere.[1-3] One of the proposed strategies to control the global warming is the development of clean sources of energy. For that reason, several energy systems are being studied and the hydrogen is presented as a promising fuel for the future. Usually, hydrogen is mainly obtained from syngas through different catalytic reactions such as dry and steam

methane reforming processes, water-gas shift reaction and others.[4–10] However, in the syngas, hydrogen is always accompanied by carbon dioxide (CO_2) or carbon monoxide (CO).[10-11] Therefore, to get high purity hydrogen, it must be separated from carbon oxides. In this regard, sorption enhanced steam methane reforming (SE-SMR) is a process which involves the catalytic steam methane reforming (SMR) and water-gas shift reaction, as well as carbon monoxide or dioxide sorption by a solid sorbent.[4,12–15] When the syngas is composed by H_2 and CO_2, there are several materials which have been already studied theoretically and experimentally as sorbents in the SE-SMR process. Some of these materials are zeolites, calcium oxide and alkaline ceramics, among others.[4,13,15–24] However, if the syngas contains CO, there are not many reported materials capable to chemisorb this gas.

In this regard, a few alkaline ceramics (lithium and sodium zirconates, sodium cobaltate and lithium cuprate)[25-29] have been studied as possible CO captors through a bifunctional process: *i*) catalyzing the carbon monoxide through an oxidizing process and *ii*) chemisorbing the produced CO_2. These reports have evidenced that these materials are able to perform the double process in a wide temperature range, and even more, the kinetics and efficiencies of the CO captured are comparable to the CO_2 capture reports, under similar physicochemical conditions. These results have opened the possibility to produce high purity H_2, from syngas by the chemical capture of carbon monoxide through this bifunctional process.

On the other hand, two different lithium ferrites have been recently proposed as CO_2 captors; $LiFeO_2$ and Li_5FeO_4 (reactions 1 and 2). These materials have a completely different behavior when they have been tested as CO_2 captors. $LiFeO_2$ is only able to trap small

amounts of CO_2 between 200 and 500 °C,[30-32] while the Li_5FeO_4 phase is able to chemisorb large amounts of CO_2 in a wide range of temperatures (between 300 and 800 °C).[33]

$$2LiFeO_2 + CO_2 \rightarrow Li_2CO_3 + Fe_2O_3 \quad (1)$$

$$Li_5FeO_4 + 2CO_2 \rightarrow 2Li_2CO_3 + LiFeO_2 \quad (2)$$

Based on this background, the aim of this work was theoretically and experimentally to evaluate the Li_5FeO_4 as a possible bifunctional material; as catalyst during the CO oxidation process and as sorbent during the subsequent CO_2 chemisorption. Moreover, since the $LiFeO_2$ phase is one of the products obtained after the CO_2 capture on Li_5FeO_4, its catalytic and chemisorption behaviors under the same physicochemical conditions was also evaluated.

Experimental section

Li_5FeO_4 was synthesized by solid state reaction.[33] Lithium oxide (Li_2O, Sigma-Aldrich) and iron (III) oxide (Fe_2O_3, Sigma-Aldrich) were mechanically mixed using a lithium excess of 20 wt.% based on the stoichiometric lithium content on the pentalithium ferrite, then the mixture was uniaxially pressed into pellets using a pressure of 15 MPa. Subsequently, the pellets were heated at 850 °C for 20 h. On the contrary, $LiFeO_2$ sample was synthesized by nitrate pyrolysis method,[32] using lithium carbonate (Li_2CO_3, MEYER), iron nitrate nona-hydrate ($Fe(NO_3)_3 \cdot 9H_2O$, MEYER) and nitric acid (HNO_3, Sigma-Aldrich), as reagents. Precursors were subsequently annealed at 500 °C (3 h), and at 670 °C (3 h), under an air atmosphere. After the synthesis, both lithium ferrites were structural and

microstructurally characterized using X-ray diffraction and N_2 adsorption as it was described in previous papers[32-33].

In order to understand the experimental results, *ab initio* thermodynamic calculations were performed by combining density functional theory (DFT) with lattice phonon dynamics.[33] The detailed descriptions of the calculation method can be found in previous studies.[34-36] The Vienna *ab-initio* simulation package (VASP)[37-38] was used to optimize the lithium ferrite solid structures, in order to obtain their DFT energies. Then, the corresponding supercells were created for phonon calculations. In the phonon calculations, displacements of 0.03Å of non-equivalent atoms were generated. After that, DFT calculations were performed, again, to obtain the force on each atom due to displacements. These forces are carried back to PHONON package[39] to calculate the phonon dispersions and densities, from which the partition function can be carried out and used to obtain free energies and entropies. From the calculated DFT energy, phonon free energy and entropy of each reactant and product, the thermodynamic properties ($\Delta H(T)$, $\Delta G(T)$, $\Delta S(T)$) of capture reactions and their temperature-CO_2 pressure relationships can be obtained and used for evaluating the reactions of this study.

To evaluate the bifunctional process in the Li_5FeO_4 and $LiFeO_2$, a thermobalance and a catalytic reactor were used, where all the experiments were performed using powders. CO chemisorption experiments were performed on a thermobalance (TA Instruments, model Q500HR) using dynamic an isothermal conditions. The experiments were carried out under two different gas mixtures: CO (5 vol % in N_2, Praxair, certificate standard) in absence or presence of O_2 (Praxair, grade 2.6). The total flow rate used was 60 mL/min. For the dynamic experiments, the samples were heated from 30 to 850 °C at a heating rate of 5 °C/min under

the different gas mixtures: *i*) P_{CO}=0.05 or *ii*) P_{CO}=0.05 and P_{O2}=0.05. For comparison purposes, a CO_2 (Praxair, grade 3.0) thermogravimetric dynamic analysis with a low partial pressure of carbon dioxide (P_{CO2}=0.1) was performed. For the isothermal analysis, the samples were heated to the specific temperature (between 500 and 700 °C) under a N_2 flux. Then, the gas flow was switched from N_2 to the corresponding gas mixture. Again, the isothermal experiments were carried out using the same total flow and gas mixture as in the dynamic experiments. It is worth noting that the isothermal analyses were performed only with the Li_5FeO_4, according to the results presented below.

For the catalytic tests, Li_5FeO_4 and $LiFeO_2$ samples were evaluated dynamically and isothermally in the CO oxidation reaction in oxygen (O_2) presence and absence, using a catalytic reactor (Bel-Japan, model Bel-Rea) with 200 mg of sample. Initially, all samples were cleaned under 50 $mL \cdot min^{-1}$ of N_2 for 10 min. Then, both lithium ferrites were dynamically heated from 30 to 900 °C at a heating rate of 2 °C/min, using the same gas mixtures described above in the thermogravimetric analyses. Only the Li_5FeO_4 sample was analyzed isothermally at 500, 550, 600, 650 and 700 °C. Li_5FeO_4 samples were cleaned and heated at 15 °C/min to the corresponding temperature under a N_2 flux. Once the corresponding temperature was reached, the flow gas was switched from N_2 to the desired gas mixture and maintained during 3 h. The course of the reaction was followed by analyzing the gas products composition in a GC-2014 gas chromatograph (Shimadzu) with a Carboxen-1000 column.

Pristine Li_5FeO_4 and products obtained after isothermal CO oxidation tests were characterized by powder X-ray diffraction (XRD), temperature programed desorption (TPD) of CO_2 and CO, and X-ray photoelectron spectroscopy (XPS). XRD patterns were recorded

in the $10^o \leq 2\theta \leq 70^o$ range, using a goniometer speed of 1^o (2θ)/min, with a diffractometer Siemens D5000 coupled to a cobalt anode (λ = 1.789 Å). TPD analyses with CO_2 and CO were performed on a chemisorption analyzer (Belcat, BelJapan). Before each analysis, about 50 mg of sample was introduced in a quartz cell and pretreated by heating the sample up to 850 °C under a He flow of 30 mL/min. Then, the sample was cooled to 200 °C and saturated with a 60 mL/min flow of CO_2 or 100 mL/min flow of CO (diluted 5 vol% in N_2) for 60 min. Afterwards, the TPD was performed by heating the sample up to 900 ºC using a ramp of 5 ºC/min in a He flow, quantifying the data by a thermal conductivity detector (TCD). Finally, electronic structure analyses were performed by XPS in an ESCA2000 Multilab equipment (VG Microtech, from UK) with UHV system, Al K X-ray (1486.6 eV) and CLAM4 MCD analyser. The sample surface was sputtered for 21 minutes with 0.33 $\mu A/mm^2$ argon ions produced at 4.5 kV. The peak positions on the XPS spectra were referenced to the C 1s core-level localized at 285.00 eV. The XPS spectra were deconvoluted using SDP v4.1 software. The curve fitting procedure for the signal analysis was as follows: i) All spectra were calibrated to the C 1s peak at 285.00 eV as carbon is ubiquitous and present on any surface; ii) the linear method for background subtraction was employed in the BE analysis range; iii) the Gaussian-Lorentzian ratio was fixed to 0.95 to simulate the peak profile; iv) the asymmetry factor was fixed to 0.2; v) the peak positions for the Fe^{3+} $2p_{3/2}$ and Fe^{3+} $2p_{1/2}$ were obtained from the first fit of the data for the x = 0 sample and then fixed for the following analyses; vi) the peak positions for the Fe^{2+} $2p_{3/2}$ and Fe^{2+} $2p_{1/2}$ were obtained from the work of McIntyre and Zetaruk;[39] vii) the full width at half maximum (FWHM) was initially determined on the original sample and then used as the initial parameter for the catalytic products and; viii) the best fit was selected by its minimum χ^2 value.

Results and discussion

Figure 1 presents the calculated thermodynamic properties of Li_5FeO_4 and $LiFeO_2$ reacting with CO-O_2 *versus* temperature, where the CO_2-lithium ferrites reaction properties are included for comparison purposes. It is evident that, in both lithium ferrites, the enthalpy heat of reaction values (ΔH) changed importantly depending if ceramic reacts with CO_2 or CO-O_2 (Figure 1-A). In fact, ΔH values were more exothermic (around 400 kJ/mol) when lithium ferrites reacted with CO-O_2, in comparison to the CO_2 cases. It can be explained due to heat released from the CO oxidation process, which is a highly exothermic reaction. Moreover, according to the Gibbs free (ΔG) energy curves, both lithium ferrites carbonations in the CO-O_2 presence are thermodynamically stable (at least up to 1100 °C), while in the CO_2 processes, only the Li_5FeO_4 is stable at high temperatures (Figure 1-B).

Based on the theoretical results showed above, different CO capture and catalytic experiments were performed. Figure 2 shows the dynamic TG experiments of Li_5FeO_4 using different gas atmospheres: $CO{-}O_2$, CO and CO_2; the last one for comparison purposes. The $Li_5FeO_4{-}CO_2$ and $Li_5FeO_4{-}CO{-}O_2$ systems presented a similar behavior as a function of temperature than those observed in other alkaline ceramics.[28,40-41] Initially, between 225 and 550 °C, both systems presented a weight increase attributed to a superficial CO-O_2 or CO_2 chemisorption processes. Moreover, the DTG curves evidenced a double process in both system reactions, which has been previously attributed to a Li_5FeO_4 partial sintering or the CO_2 chemisorption-desorption process of $LiFeO_2$.[32-33] After that, both thermograms presented a second weight increment between 600 and 700 °C, corresponding to the CO_2 or

CO-O_2 bulk chemisorptions. These results confirmed that Li_5FeO_4 is able to chemisorb CO in a similar way than CO_2. Nevertheless, oxygen must be present during the CO chemisorption process; otherwise, the CO chemisorption is significantly modified. In the oxygen absence, the TG general trend followed the same behavior. However, the superficial and bulk CO chemisorptions were highly reduced, followed by a significant desorption process between 750 and 850 °C. Variations observed in the presence or absence of oxygen must be highly related to the oxygen availability during the CO oxidation-chemisorption mechanism, as in the oxygen gas absence it has to be obtained from the Li_5FeO_4 crystalline structure.

In order to further analyze the CO oxidation and subsequent CO_2 chemisorption, different isothermal experiments were performed into the TG equipment using CO-O_2 (350-800 °C) and CO (600-750 °C) gas flows (Figure 3). In the CO-O_2 case (Figure 3-A), the first two isotherms, performed at the lowest temperatures (350 and 400 °C), only gained 5.0 and 8.0 wt.% following a typical increasing trend. However, the isotherms performed between 450 and 500 °C decreased the final weight increments to 7.4 and 4.4 wt.%, respectively. This atypical trend is in good agreement with the double CO-O_2 chemisorption observed on the dynamic TG curve. Thus, isotherms confirm the sintering and $LiFeO_2$-CO_2 desorption processes. At higher temperatures (up to 750 °C), all the isotherms presented an increasing trend. While isotherm performed at 600 °C gained 12.5 wt.% after 3 h, the final weight increment at 750 °C was equal to 48.6 wt.%. When the isotherm was performed at 800 °C, the final weight increment was slightly reduced (43.0 wt.%), in comparison to the isotherm performed at 750 °C, due to the CO_2 desorption activation. It should be pointed out that at the first moments (600 s), CO-O_2 chemisorption isotherms performed between 500 and 800

°C presented faster weight increments, indicating that these isotherms presented a faster kinetic capture.

Then, in order to complement this analysis, a second set of isothermal experiments were performed in the absence of oxygen (Figure 3-B). Under these gas conditions, isotherms presented smaller weight increments at almost all the temperatures, except at 700 °C. These results must be attributed to the oxygen availability and CO_2 chemisorption-desorption equilibrium, which must be highly related to the lack of CO_2 in the gas flow. However, at 700 °C the final weight increment was 40.0 wt.% in the oxygen absence, while in the oxygen presence the weight increment was only 33.0 wt.%, it means 7.0 wt.% less.

Although the CO chemisorption, in oxygen absence, was not as high as in the oxygen presence, these results confirms that Li_5FeO_4 is able to release some oxygen atoms from its crystalline structure for the Li_2CO_3 formation. In such a case, Fe^{3+} must be reduced to Fe^{2+} or even Fe^0.

After the thermogravimetric analysis, the CO-O_2 and CO reactivity with Li_5FeO_4 were further evaluated into a catalytic reactor connected to a gas chromatograph (Figures 4-6). In the CO-O_2 case, CO and O_2 conversion began at around 300-320 °C, continuing between 400-710 °C and 800-900 °C (Figure 4-A). The CO oxidation produced by Li_5FeO_4 was correlated to the CO_2 production in the same temperature ranges. Additionally, these temperature ranges are in good agreement with the weight increments observed previously in the thermogravimetric analysis. Moreover, these results indicate that only part of the CO_2 produced is being chemically trapped in the Li_5FeO_4 sample, otherwise no CO_2 could be detected by GC.

The same Figure 4-A shows different gas evolution trends at higher temperatures than 700 °C. Between 700 and 720 °C the CO oxidation seemed to be suddenly reduced. This temperature fits very well with the Li_2CO_3 decomposition temperature, 720 °C.[42-43] Thus, the CO_2 desorption must inhibit the CO oxidation. Later at higher temperatures than 720 °C, once the Li_2CO_3 was decomposed, the CO oxidation was reactivated, producing CO_2, which was not chemisorbed on Li_5FeO_4 due to temperature.

In general, when the catalytic test was performed in the oxygen absence (Figure 4-B) the thermal behavior was similar to that observed on the oxygen presence. However, the CO conversion and CO_2 production were significantly lower, as it could be expected. Moreover, the CO conversion showed three very specific behaviors at different temperature ranges. Initially, between 300 and 415 °C it was produced a small CO decrement, without any CO_2 detection. Then, between 415 and 710 °C the CO conversion and CO_2 production presented the highest catalytic activity. Finally, at temperatures higher than 710 °C the CO oxidation tended to decrease totally, while the CO_2 production continued. In fact, in this temperature range the CO amounts detected were higher than 100 %. These specific behaviors fit well with three processes: 1) the CO oxidation, 2) CO_2 superficial (300-415 °C) and CO_2 partial bulk chemisorptions (415-710 °C), and 3) finally to the desorption process (T > 710 °C), where all the gas is desorbed as a mixture of CO and CO_2.

Based in all previous results two set of isothermal experiments were performed, in presence and absence of oxygen. In the CO-O_2 case (Figure 5), at 500 °C, the CO conversion and CO_2 production isotherms exhibited poor catalytic performance, around 22-30 %. Then, for the isotherms performed between 550 and 600 °C, the CO conversion presented the highest efficiencies (71-92 %). In these cases, the CO_2 productions were the highest, as it

could be expected considering TGA results (Figures 2 and 3), but the CO_2 amounts (~60 %) did not fit with the CO evolution. The variation observed between these two gases is related to the CO_2 chemisorbed in Li_5FeO_4. Then, isotherms performed at higher temperatures than 600 °C showed a decrease in the catalytic behavior of the CO oxidation, which must be related to the catalytic inactivation produced by the fast Li_5FeO_4 carbonation.

When these isothermal experiments were performed in the absence of oxygen (Figure 6), isotherms showed similar CO oxidation conversions and CO_2 productions, but with a different thermal trend. In this case, the CO oxidation increased as a function of temperature during the first hour, then the CO oxidation tended to decrease. In fact, the highest decrement was observed on the isotherm performed at 650 °C. At the same time, the CO_2 production increased as a function of temperature, where the highest production was obtained at 700 °C, although it decreases after 3 h. After the isothermal experiments, some of the final Li_5FeO_4 solid products were analyzed by XRD and XPS in order to confirm the carbonation process and to determine the secondary phase evolution. Additionally, TPD experiments of CO_2 and CO were performed on Li_5FeO_4 to better understand the reaction mechanism.

Figure 7 shows the XRD patterns of pristine Li_5FeO_4 and products obtained after the isothermal experiments at different temperatures, in presence and absence of oxygen. In the presence of oxygen, in addition to Li_5FeO_4, two other phases ($LiFeO_2$ and Li_2CO_3) were always detected, independently of the temperature. This result is in good agreement with the reaction 3.

$$Li_5FeO_4 + 2CO + O_2 \rightarrow LiFeO_2 + 2Li_2CO_3 \qquad (3)$$

However, when the isothermal experiments were performed in the absence of oxygen, the final products were Li_5FeO_4 as unreacted material, $LiFeO_2$, Li_2CO_3 and metallic iron (Fe^0). The presence of Fe^0 indicates that part of the oxygen present in the lithium ferrites (Li_5FeO_4 and/or $LiFeO_2$) is being released for the CO oxidation process. This process cannot be subscribed as a direct reaction, as in such a case iron and lithium metals should be produced. However, a partial lithium ferrites reduction may have taken place (reactions 4 and 5), with a subsequent $LiFeO_2$ or $Li(Fe^{3+}_{1-2x}Fe^{2+}_{2x})O_{2-x}$ reduction.

$$Li_5(Fe^{3+})O_4 + x\ CO \rightarrow Li_5(Fe^{3+}_{1-2x}Fe^{2+}_{2x})O_{4-x} + x\ CO_2 \qquad (4)$$

$$2\ Li(Fe^{3+})O_2 + x\ CO \rightarrow 2\ Li(Fe^{3+}_{1-2x}Fe^{2+}_{2x})O_{2-x} + x\ CO_2 \qquad (5)$$

Therefore, assuming that Li_5FeO_4 initially evolves to Li_2CO_3 and $LiFeO_2$, being $LiFeO_2$ the reducible specie, the metallic iron formation must be produced according to any of the following reactions (reactions 6, 7 or consecutive reactions 8 and 9):

$$2LiFeO_2 + CO \rightarrow Li_2CO_3 + 2Fe + O_2 \qquad (6)$$

$$2LiFeO_2 + 3CO \rightarrow Li_2CO_3 + 2Fe + 2CO_2 \qquad (7)$$

$$2LiFeO_2 + CO \rightarrow Li_2CO_3 + 2FeO \qquad (8)$$

$$FeO + CO \rightarrow Fe + CO_2 \qquad (9)$$

In the present work, gas chromatograph results did not evidence the oxygen release, but in a previous work performed for the CO oxidation and capture on sodium cobaltate ($NaCoO_2$),[26] the oxygen release was observed during the cobalt partial reduction (similar to reaction 6). However, if the CO concentration is high enough iron reduction would be possible with a CO_2 release (reaction 7). Finally, another possibility for the iron reduction implies a double step mechanism, where $LiFeO_2$ reacts with CO, producing Li_2CO_3 and FeO

(where Fe is partially reduced from Fe^{3+} to Fe^{2+}, reaction 8) and later FeO may continue reacting with CO to produce Fe^0 and CO_2 (reaction 9).

To elucidate and confirm any of the reaction evolutions previously suggested, TPD and XPS experiments were performed on Li_5FeO_4 as well as different gravimetric and catalytic experiments with the $LiFeO_2$-CO and $LiFeO_2$-CO-O_2 systems. Finally, different thermodynamic properties were calculated for the proposed $LiFeO_2$-CO reacting systems. The Li_5FeO_4 was characterized by CO_2 and CO TPD (Figure 8). The CO_2 profile showed two important desorption steps, the first between 250 and 315 °C, which was associated to a superficial chemisorption (weakly-bound CO_2). The second and highest desorption was observed between 480 and 640 °C and it may be attributed to a stronger bounded adsorption. On the other hand, the CO profile presented a very narrow similar trend than that previously described for CO_2, which suggests that CO is not adsorbed on Li_5FeO_4.

Figure 9 shows the deconvoluted Fe 2p XPS spectra of the pristine Li_5FeO_4 (A), and two different Li_5FeO_4 isothermal catalytic products; the CO-O_2 (B) and CO (C) isotherms performed at 700 °C. Pristine Li_5FeO_4 spectrum presents the characteristic $2p_{3/2}$ and $2p_{1/2}$ peaks at 710.67 and 724.77 eV, respectively. These values confirm the presence of Fe^{3+} in the sample, as it could be expected. The spectrum of the Li_5FeO_4-CO-O_2 oxidation product presents the same peaks of $2p_{3/2}$ and $2p_{1/2}$ signals at 710.67 and 724.77 eV respectively indicating the same oxidation state for iron than that observed in the pristine Li_5FeO_4. In this case, a third peak was deconvoluted at 719.23 eV, which was associated with the satellite peak of the Fe $2p_{3/2}$ signal. Thus, the CO-O_2 flow does not modify the electronic structure of Fe in the sample, although the CO oxidation and CO_2 capture processes were produced. On the other hand, the spectra obtained for the Li_5FeO_4-CO isotherm presents a slightly different

profile, which was shifted to lower energies. First, the Fe $2p_{3/2}$ and $2p_{1/2}$ signals were shifted to 708.18 and 720.24 eV respectively, and those signals are associated with Fe^{2+}.[32] Moreover, another peak was located at 704.7 eV, which is consistent with the presence of metallic Fe in the material. These features agree with the previous result where the presence of metallic Fe was confirmed by XRD in the same sample. In this case, the CO reduces the Li_5FeO_4 phase to form Li_2CO_3 and metallic Fe, and the presence of partially reduced lithium ferrites phases with Fe^{2+} are proposed, as intermediates, according to reactions 4, 5 and 8.

In order to complement all the Li_5FeO_4 results and to elucidate the $LiFeO_2$ influence in the CO-O_2 oxidation-chemisorption on Li_5FeO_4, different thermogravimentric and catalytic analyses were performed on $LiFeO_2$ using CO-O_2 or CO gas mixtures (Figure 10). During the thermogravimetric analysis, the $LiFeO_2$-CO-O_2 system did not show important weight changes, and by the end of the experiment only a negligible 0.2 wt.% decrement took place. On the other hand, the $LiFeO_2$-CO system did not present any weight changes up to 380 °C. After that, between 380 and 620 °C, the thermograms presented a weight increase of 4.2 wt.%, which may be associated to a partial CO oxidation and subsequent CO_2 chemisorption. At temperatures higher than 620 °C, the sample presented a continuous weight decrease up to 900 °C, equivalent to 7.4 wt.%, which represents a bigger decrement than the increment previously registered. This behavior may be associated to three different processes: *i*) loss of intercrystalline O_2 used to form the CO_2, *ii*) desorption of adsorbed CO and *iii*) sample decarbonation. Additionally, the $LiFeO_2$-CO-O_2 and $LiFeO_2$-CO reactivity systems were evaluated in a catalytic reactor (Figure 10-B). In the $LiFeO_2$-CO-O_2 system, the CO and O_2 conversion began at 280 °C, reaching a 100 % conversion at 480 °C, which remained constant until 900 °C. The CO_2 production is observed in the same temperature

range and, as the CO conversion, it does not vary for the rest of the experiment. This result shows that while the $LiFeO_2$ is able to catalyze the CO oxidation, it is not able to capture the produced CO_2 in the oxygen presence and then the above result was thermodynamically confirmed (see Figure 11). The same figure 10-B shows the CO and CO_2 evolution in the absence of oxygen. In this case, the CO conversion and CO_2 chemisorption began at higher temperatures (400 °C), in comparison to the CO-O_2 case, and presented a lower maximum conversion (40 %). At T > 550 °C, the CO conversion began to decrease and so did the CO_2 production, but at a slower rate, and at T > 760 °C the concentration was higher than 100 %, while still detecting CO_2. This behavior fits well with the CO thermogravimetric analysis, where at T > 620 °C there is a continuous decrement of weight. Additionally, the catalytic reactor products were characterized by XRD (data not shown). The $LiFeO_2$-CO-O_2 product showed that the $LiFeO_2$ phase is preserved after the catalytic conversion. On the other hand, in the $LiFeO_2$-CO catalytic product, the $LiFeO_2$ phase was still observed, nevertheless the presence of Li_2CO_3 and metallic Fe was also detected, as suggested by reactions 7-9. Results described above clearly show that although a chemical transformation from Li_5FeO_4 to $LiFeO_2$ occurs at T ~ 700 °C in the Li_5FeO_4-CO-O_2 and Li_5FeO_4-CO systems, the $LiFeO_2$ subproduct is able to continue the CO_2 formation through the CO oxidation reaction at high temperatures (700-900 °C), regardless of the oxygen presence or absence. Moreover, these results confirm the presence of iron with different oxidation states (Fe^{3+}, Fe^{2+} and Fe^0). However, these results would not be conclusive about the iron reduction mechanism. Thus, different thermodynamic calculations were performed (Figure 11), trying to elucidate the correct $LiFeO_2$-CO reaction mechanism, ending with the metallic iron formation. From these results, it is more than evident that $LiFeO_2$ carbonation, with a direct iron reduction from Fe^{2+} to Fe^0 and O_2 release, is not thermodynamically favored as it was previously suggested in

reaction 6. On the other hand, reaction 7 or subsequent reactions 8 and 9 are thermodynamically favored. Nevertheless, according to the heat of reaction and Gibbs energy free curves, reaction 8 is thermodynamically favored over the subsequent reaction 8 and 9. In such a case, the iron detection is corroborated using this reaction mechanism, while the Fe^{2+} (evidenced by XPS) may be explained by the $Li_5(Fe^{3+}_{1-2x}Fe^{2+}_{2x})O_{4-x}$ but mainly $Li(Fe^{3+}_{1-2x}Fe^{2+}_{2x})O_{2-x}$ phases (see reactions 4 and 5).

Summarizing thermogravimetric and catalytic results, it can be established that Li_5FeO_4 presented interesting behavior as CO oxidant, in the presence or absence of oxygen and as a subsequent CO_2 chemisorbent. On the other hand, $LiFeO_2$ seems to present good catalytic properties by itself or as a Li_5FeO_4 carbonation secondary phase. Within this context, there are only a few reports or lithium-sodium ceramics bifunctional CO oxidants and CO_2 chemisorbents.[25-26,29] In the present case, Li_5FeO_4 presented better oxidative and sorption properties, talking about kinetic and efficiency, than lithium or sodium zirconates (Li_2ZrO_3 or Na_2ZrO_3) or sodium cobaltate ($NaCoO_2$), but similar properties than lithium cuprate (Li_2CuO_2). However, it has to be mentioned that CO conversion and chemisorption capacity of Li_5FeO_4 (12.9 $mmol_{CO2}/g$) is higher than that of Li_2CuO_2 (9.1 $mmol_{CO2}/g$), due to the lithium amounts on each ceramic. Furthermore, Li_5FeO_4 and Li_2CuO_2 are able to release oxygen atoms from their crystalline structures to facilitate the CO oxidation process, with the corresponding iron or cooper reduction processes. Base on that, it may be possible to continue working the lithium ferrites as bifunctional materials, which may be used in different industrial processes, such as the syngas separation and H_2 enrichment.

Conclusions

Two lithium ferrites (Li_5FeO_4 and $LiFeO_2$) were synthetized, characterized and tested as possible catalytic and subsequent captor materials, for the double bifunctional process of CO oxidation and CO_2 chemisorption. Both materials were evaluated thermogravimetric and catalytically using two different gas flows: CO or CO-O_2. Li_5FeO_4 and $LiFeO_2$ were able to perform the CO oxidation and CO_2 chemical capture. In fact, according to XRD, TGA and catalytic analyses, $LiFeO_2$ is produced as a secondary product phase of the Li_5FeO_4 carbonation, continuing the CO oxidation process and the CO_2 capture at T > 700 °C, regardless the O_2 absence or presence, being its higher contribution in the CO-O_2 system. The bifunctional process was confirmed by the lithium ferrites carbonation and formation of other secondary phases. In the oxygen absence, the CO oxidation was produced by the oxygen release from the lithium ferrites crystalline structures, assisted by the partial iron reduction, from Fe^{3+} to Fe^{2+} or even more to Fe^0.

As it could be expected, the oxidation and chemisorption processes varied as a function of the lithium ferrite type and oxygen content. Li_5FeO_4 was able to perform both processes in presence and absence of oxygen. During the catalytic tests, this lithium ferrite presented the best CO oxidation results at 500 °C, independently of the oxygen presence or absence. On the contrary, the best CO_2 chemisorptions on Li_5FeO_4 were observed at 750 and 700 °C with or without oxygen, respectively. On the contrary, CO oxidation using $LiFeO_2$ presented a good catalytic CO oxidation in the oxygen presence. Under these conditions, the CO oxidation starts from 500 °C, but the CO_2 chemisorption was only occurred in the oxygen absence. Based on these results, different reaction mechanisms were proposed for each lithium ferrite and they were corroborated through the catalyst characterizations (TGA, TPD and XPS) and different thermodynamic calculations.

Acknowledgements

H. A. Lara-García and E. Vera thank to CONACYT, while J. A. Mendoza-Nieto and J. F. Gómez-García thank to DGAPA-UNAM for personal financial supports. The present work was financially supported by the projects SENER-CONACYT (251801) and PAPIIT-UNAM (IN-101916). Finally, authors thank to A. Tejeda and L. Huerta for technical assistant.

References

(1) IPCC, CLIMATE CHANGE 2001 : Impacts , adaptation and vulnerability. Work. Gr. II Impacts Adapt. vulnerability 2001, 10.

(2) J. C. Abanades, B. Arias, A. Lyngfelt, T. Mattisson, D. E. Wiley, H. Li, M. T. Ho, E. Mangano, S. Brandani, Inter. J. Greenh. Gas Control 40 (2015) 126.

(3) J. Wang, L. Huang, R. Yang, Z. Zhang, J. Wu, Y. Gao, Q. Wang, D. O'Hare, Z. Zhong, Energy Environ. Sci. 7 (2014) 3478.

(4) A. Lopez Ortiz, D. P. Harrison, Ind. Eng. Chem. Res 40 (2001) 5102.

(5) Y. N. Wang, A. E. Rodrigues, Fuel 84 (2005) 1778.

(6) S. Saeidia, F. Fazlollahic, S. Najarid, D. Iranshahib, J. Jaromír L. L. B. Klemeše, J. Ind. Eng. Chem. 49 (2017) 1.

(7) A. López Ortiz, M. J. Meléndez, V. C. M. Zaragoza, Inter. J. Hydrogen Energy 41 (2016) 23363.

(8) B. Dou, Y. Song, C. Wang, H. Chen, Y. Xu, Renew. Sustain. Energy Rev. 30 (2014) 950.

(9) S. Wang, G. Q. Lu, G. J. Millar, Energy & Fuels 10 (1996) 896.

(10) R. Chaubey, S. Sahu, O. O. James, S. Maity, Renew. Sustain. Energy Rev. 23 (2013) 443.

(11) M. Farniaei, M. Abbasi, H. Rahnama, M. R. Rahimpour, A. Shariati, J. Nat. Gas Sci. Eng. 20 (2014) 132.

(12) Y. Chen, Y. Zhao, J. Zhang, C. Zheng, Sci. China Technol. Sci. 54 (2011) 2999.

(13) H. K. Rusten, E. Ochoa-Fernández, H. Lindborg, D. Chen, H. A. Jakobsen, Ind. Eng. Chem. Res. 46 (2007) 8729.

(14) M. H. Halabi, M. H. J. M. de Croon, J. van der Schaaf, P. D. Cobden, J. C. Schouten, Chem. Eng. J. 168 (2011) 872.

(15) D. P. Harrison, Ind. Eng. Chem. Res. 47 (2008) 6486.

(16) K. D. Dewoolkar, P. D. Vaidya, Inter. J. Hydrogen Energy 41 (2016) 6094.

(17) I. Aloisi, N. Jand, S. Stendardo, P. Ugo-Foscolo, Chem. Eng. Sci. 149 (2016) 22.

(18) J. Phromprasit, J. Powell, S. Wongsakulphasatch, W. Kiatkittipong, P. Bumroongsakulsawat, S. Assabumrungrat, Chem. Eng. J. 313 (2017) 1415.

(19) K. B. Yi, D. P. Harrison, Ind. Eng. Chem. Res. 44 (2005) 1665.

(20) C. Wang, B. Dou, B. Jiang, Y. Song, B. Du, C. Zhang, K. Wang, H. Chen, Y. Xu, Inter. J. Hydrogen Energy 40 (2015) 7037.

(21) R. Delmelle, R. B. Duarte, T. Franken, D. Burnat, L. Holzer, Inter. J. Hydrogen Energy 41 (2016) 20185.

(22) E. Ochoa-Fernández, H. K. Rusten, H. A. Jakobsen, M. Rønning, A. Holmen, D. Chen. Catal. Today 106 (2005) 41.

(23) Y. Ding, E. Alpay, Chem. Eng. Sci. 55 (2000) 3929.

(24) E. Ochoa-Fernández, G. Haugen, T. Zhao, M. Rønning, I. Aartun, B. Børresen, E. Rytter, M. Rønnekleiv, D. Chen, Green Chem. 9 (2007) 654.

(25) H. A. Lara-García, B. Alcántar-Vázquez, Y. Duan, H. Pfeiffer, J. Phys. Chem. C 120 (2016) 3798.

(26) E. Vera, B. Alcántar-Vázquez, Y. Duan, H. Pfeiffer, RSC Adv. 6 (2016) 2162.

(27) B. Alcántar-Vázquez, E. Vera, F. Buitron-Cabrera, H. A. Lara-García, H. Pfeiffer, Chem. Lett. 44 (2015) 480.

(28) E. Vera, B. Alcántar-Vázquez, H. Pfeiffer, Chem. Eng. J. 271 (2015) 106.

(29) B. Alcántar-Vázquez, Y. Duan, H. Pfeiffer, Ind. Eng. Chem. Res. 55 (2016) 9880.

(30) I. Yanase, A. Kameyama, H. Kobayashi, J. Ceram. Soc. Japan 118 (2010) 48.

(31) M. Kato, K. Essaki, K. Nakagawa, Y. Suyama, K. Terasaka, J. Ceram. Soc. Japan 113 (2005) 684.

(32) J. F. Gomez-García, H. Pfeiffer, RSC Adv. 6 (2016) 112040.

(33) H. A. Lara-García, P. Sanchez-Camacho, Y. Duan, J. Ortiz-Landeros, H. Pfeiffer, J. Phys. Chem. C 121 (2017) 3455.

(34) Y. Duan, D. C. Sorescu, Phys. Rev. B 79 (2009) 014301.

(35) Y. Duan, Front. Environ. Sci. 3(2015) 69.

(36) Y. Duan, J. Lekse, X. Wang, B. Li, B. Alcantar-Vazquez, H. Pfeiffer, J. W. Halley, Phys. Rev. Appl., 3 (2015) 044013.

(37) G. Kresse, J. Hafner, Phys. Rev. B 47 (1993) 558.

(38) G. Kresse, J. Furthmuller, Comp. Mater. Sci. 6 (1996) 15.

(39) K. Parlinski, Software PHONON 2010.

(40) N. S. McIntyre, D. G. Zetaruk, Anal. Chem. 49 (1977) 1521.

(41) H. A. Lara-García, H. Pfeiffer, Chem. Eng. J. 313 (2017) 1288.

(42) J. W. Kim, H. G. Lee, Metall. Mater. Trans. B 32 (2001) 17.

(43) J. W. Kim, Y. D. Lee, H. G. Lee, ISIJ Inter. J. 44 (2004) 334.

Figure Captions

Figure 1. Thermodynamic properties of Li_5FeO_4 and $LiFeO_2$ reacting with $CO\text{-}O_2$ or CO_2 *versus* temperatures. (A) heat of reaction and (B) Gibbs free energy.

Figure 2. Dynamic TG and DTG curves of the $CO\text{-}O_2$, CO and CO_2 (for comparison purposes using a $P_{CO2} = 0.1$) captures for Li_5FeO_4.

Figure 3. $CO\text{-}O_2$ and CO thermogravimetric isothermal analyses of Li_5FeO_4 at different temperatures.

Figure 4. Dynamic thermal evolution of $CO\text{-}O_2\text{-}CO_2$ (A) or $CO\text{-}CO_2$ (B) using Li_5FeO_4 as a catalyst-sorbent.

Figure 5. CO evolution (A) and CO_2 formation (B) isothermal analyses of Li_5FeO_4 as catalyst, in the presence of oxygen at different temperatures.

Figure 6. CO evolution (A) and CO_2 formation (B) isothermal analyses of Li_5FeO_4 as catalyst, in the absence of oxygen at different temperatures.

Figure 7. XRD patterns of pristine Li_5FeO_4 and its isothermal catalytic products, after being treated at different temperatures, in the oxygen presence (A) or absence (B).

Figure 8. CO- and CO_2-TPD profiles of Li_5FeO_4 catalyst-sorbent.

Figure 9. XPS spectra of the Fe 2p for the pristine Li_5FeO_4 sample (A) and the Li_5FeO_4 isothermal catalytic products performed at 700 °C in the presence (B) or absence (C) of O_2.

Figure 10. Dynamic TG curves of the CO-O_2 and CO captures for $LiFeO_2$ (A) and dynamic thermal evolution of CO-O_2-CO_2 or CO-CO_2 using $LiFeO_2$ as a catalyst-sorbent (B).

Figure 11. Thermodynamic properties of different $LiFeO_2$-CO reaction mechanisms versus temperatures. (A) heat of reaction and (B) Gibbs free energy.

Figure 1

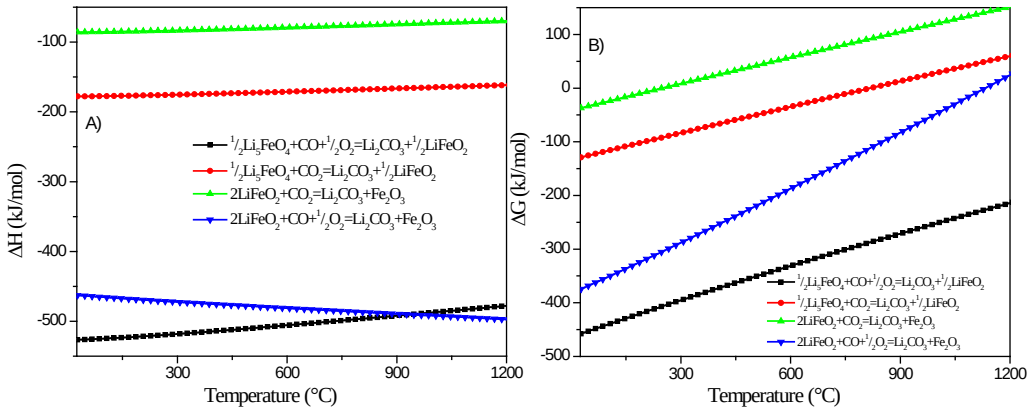
A)
B)
ΔH (kJ/mol)
ΔG (kJ/mol)
Temperature (°C)
Temperature (°C)
-100
-200
-300
-400
-500
100
0
300
600
900
1200
1/2Li5FeO4+CO+1/2O2=Li2CO3+1/2LiFeO2
1/2Li5FeO4+CO2=Li2CO3+1/2LiFeO2
2LiFeO2+CO2=Li2CO3+Fe2O3
2LiFeO2+CO+1/2O2=Li2CO3+Fe2O3

Figure 2

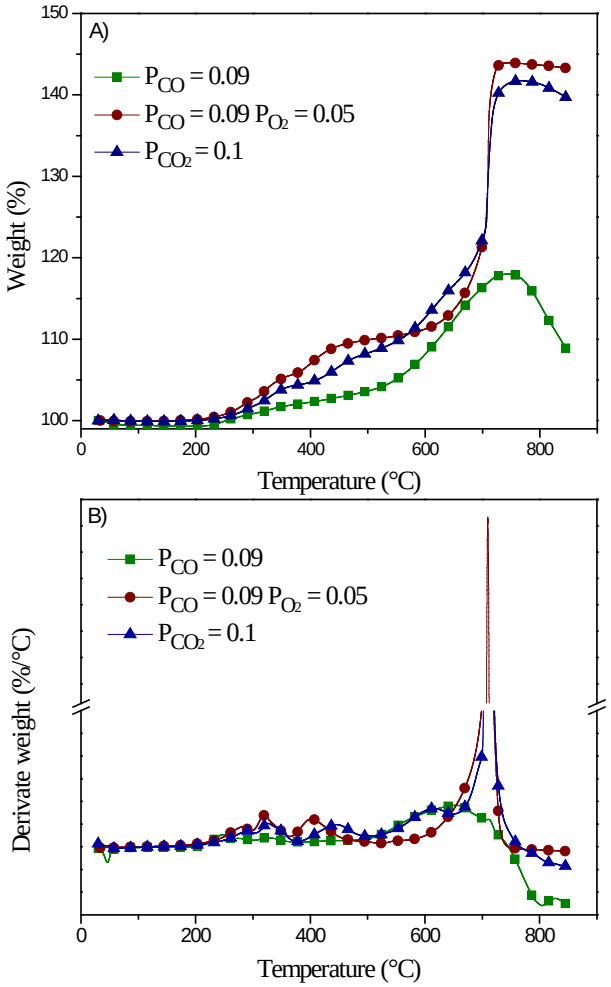
A)
P_{CO} = 0.09
P_{CO} = 0.09 P_{O_2} = 0.05
P_{CO_2} = 0.1
Weight (%)
Temperature (°C)
B)
P_{CO} = 0.09
P_{CO} = 0.09 P_{O_2} = 0.05
P_{CO_2} = 0.1
Derivate weight (%/°C)
Temperature (°C)

Figure 3

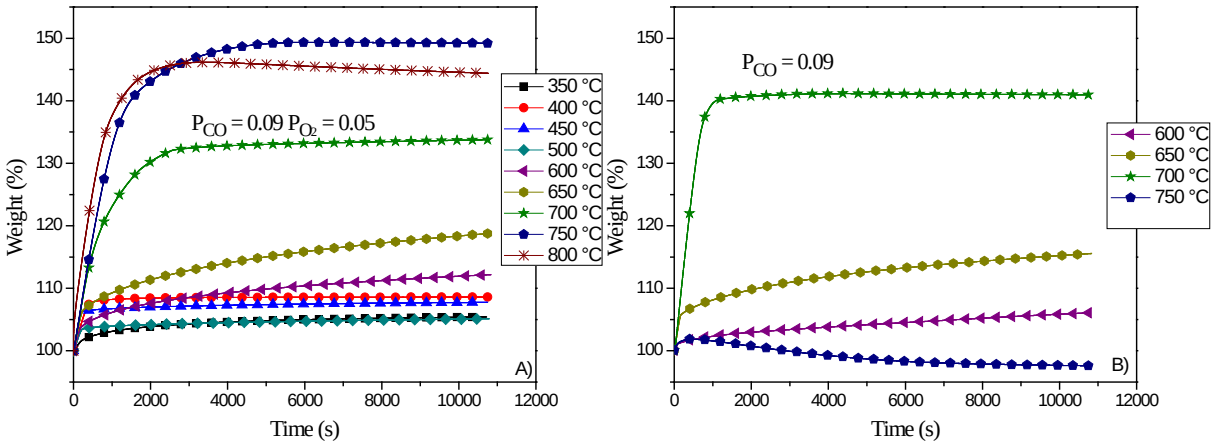
Weight (%)
Time (s)
P_{CO} = 0.09 P_{O_2} = 0.05
350 °C
400 °C
450 °C
500 °C
600 °C
650 °C
700 °C
750 °C
800 °C
A)
P_{CO} = 0.09
600 °C
650 °C
700 °C
750 °C
B)

Figure 4

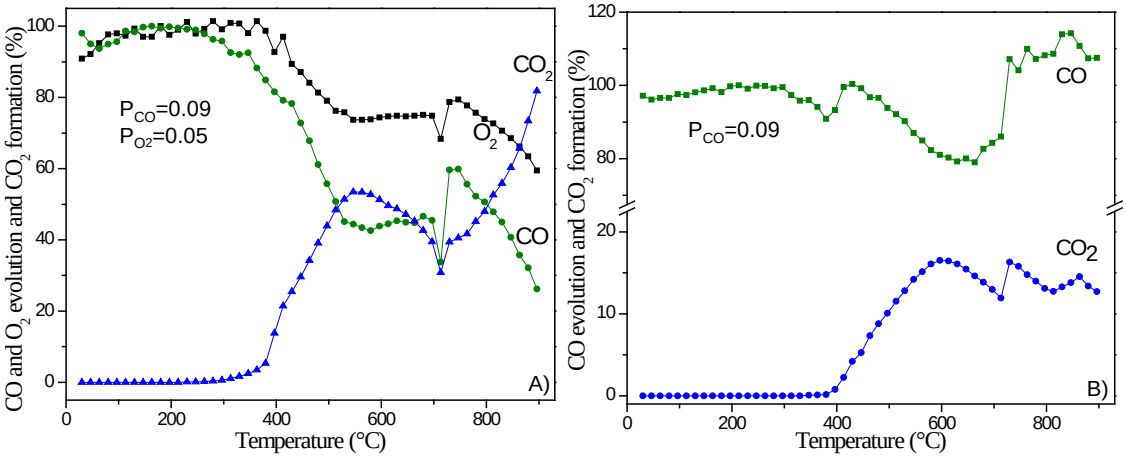
CO and O2 evolution and CO2 formation (%)
Temperature (°C)
PCO=0.09
PO2=0.05
CO2
O2
CO
A)
CO evolution and CO2 formation (%)
PCO=0.09
CO
CO2
B)

Figure 5

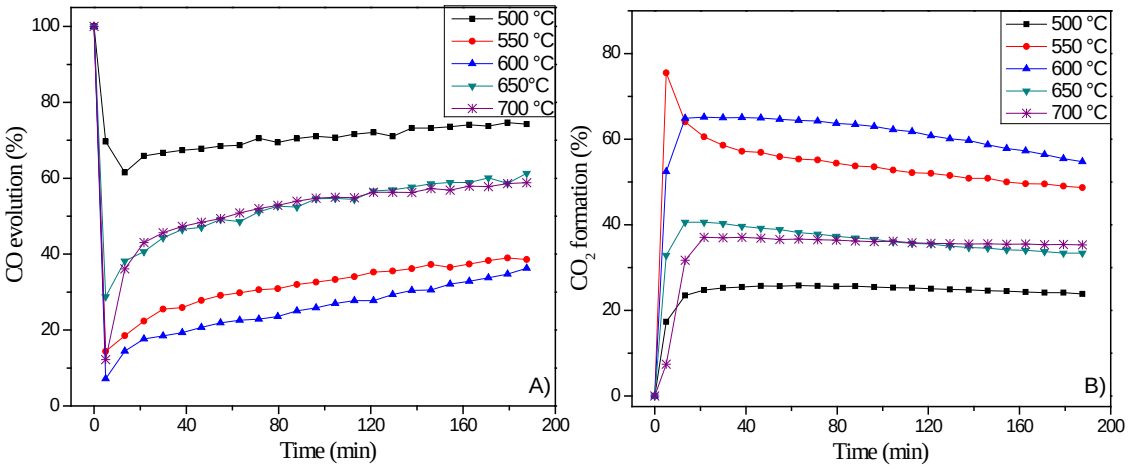
500 °C
550 °C
600 °C
650°C
700 °C
CO evolution (%)
Time (min)
A)
500 °C
550 °C
600 °C
650 °C
700 °C
CO_2 formation (%)
Time (min)
B)

Figure 6

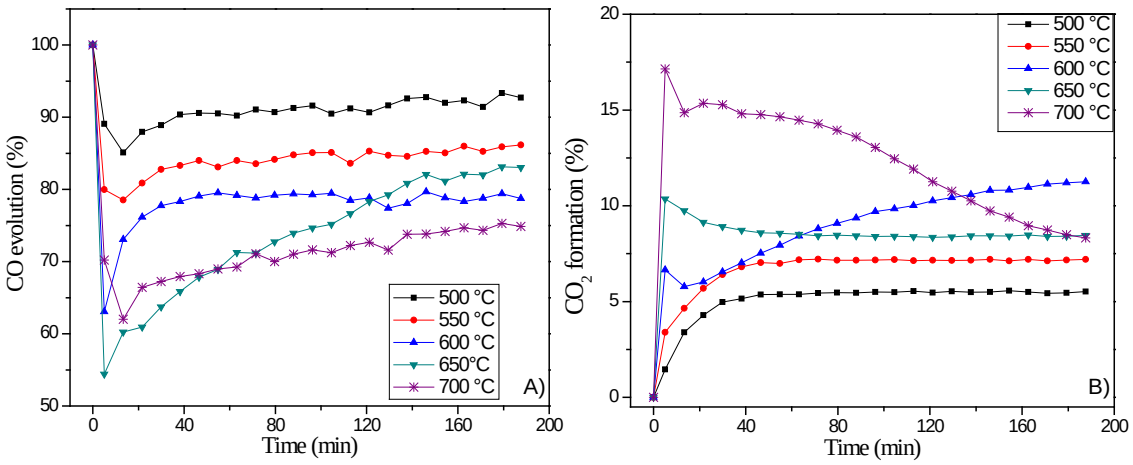
CO evolution (%)
Time (min)
500 °C
550 °C
600 °C
650°C
700 °C
A)
CO_2 formation (%)
Time (min)
500 °C
550 °C
600 °C
650 °C
700 °C
B)

Figure 7

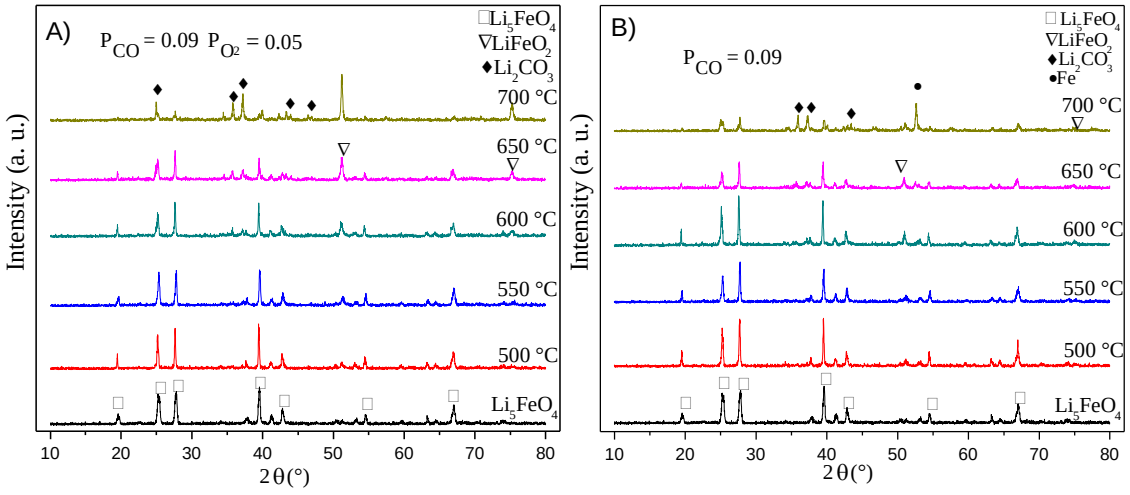
A)
P_CO = 0.09 P_O2 = 0.05
□Li5FeO4
∇LiFeO2
♦Li2CO3
700 °C
650 °C
600 °C
550 °C
500 °C
Li5FeO4
Intensity (a. u.)
2θ(°)
B)
P_CO = 0.09
□Li5FeO4
∇LiFeO2
♦Li2CO3
•Fe
700 °C
650 °C
600 °C
550 °C
500 °C
Li5FeO4
Intensity (a. u.)
2θ(°)

Figure 8

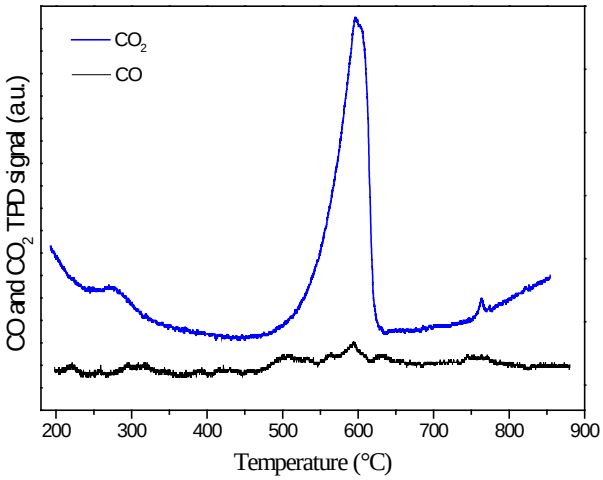
CO2
CO
CO and CO2 TPD signal (a.u.)
200
300
400
500
600
700
800
900
Temperature (°C)

Figure 9

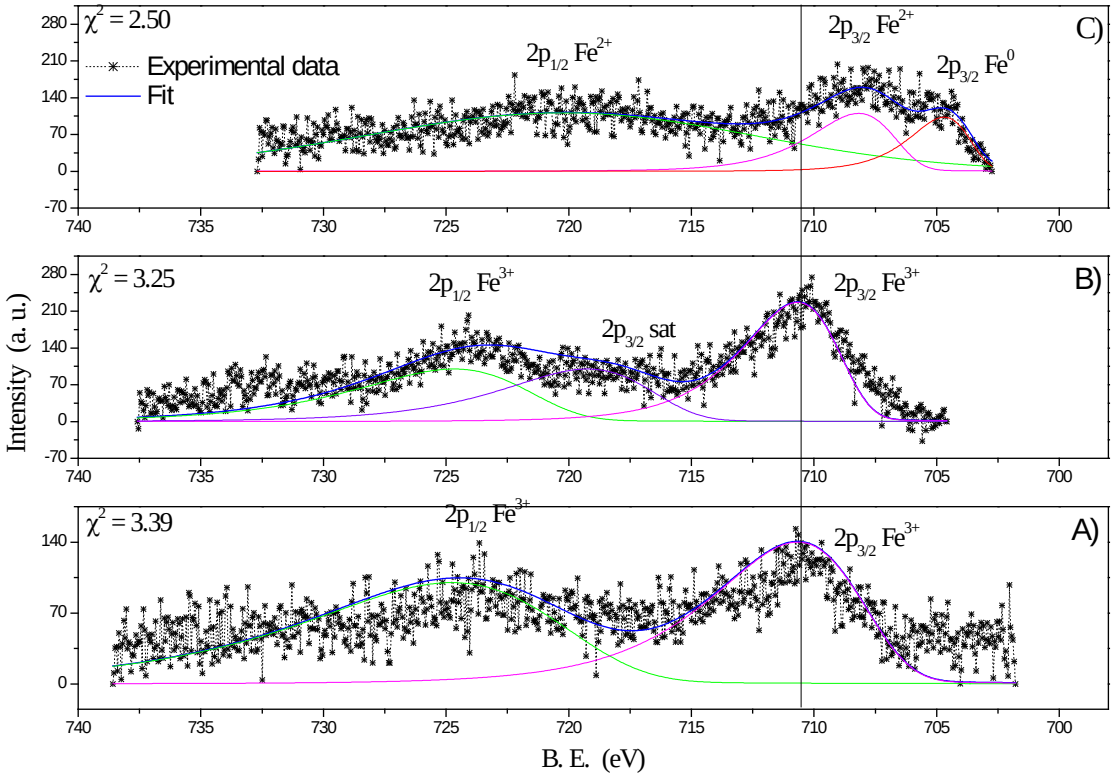
χ² = 2.50
Experimental data
Fit
2p1/2 Fe2+
2p3/2 Fe2+
2p3/2 Fe0
C)
χ² = 3.25
2p1/2 Fe3+
2p3/2 sat
2p3/2 Fe3+
B)
χ² = 3.39
2p1/2 Fe3+
2p3/2 Fe3+
A)
Intensity (a. u.)
B. E. (eV)

Figure 10

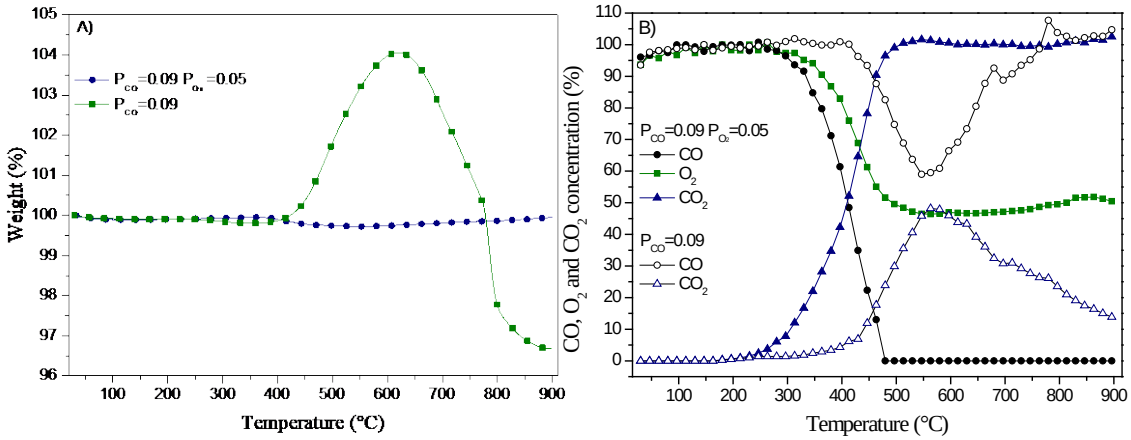
A)
P_{CO}=0.09 P_{O_2}=0.05
P_{CO}=0.09
Weight (%)
Temperature (°C)
B)
P_{CO}=0.09 P_{O_2}=0.05
CO
O_2
CO_2
P_{CO}=0.09
CO
CO_2
CO, O_2 and CO_2 concentration (%)
Temperature (°C)

Figure 11

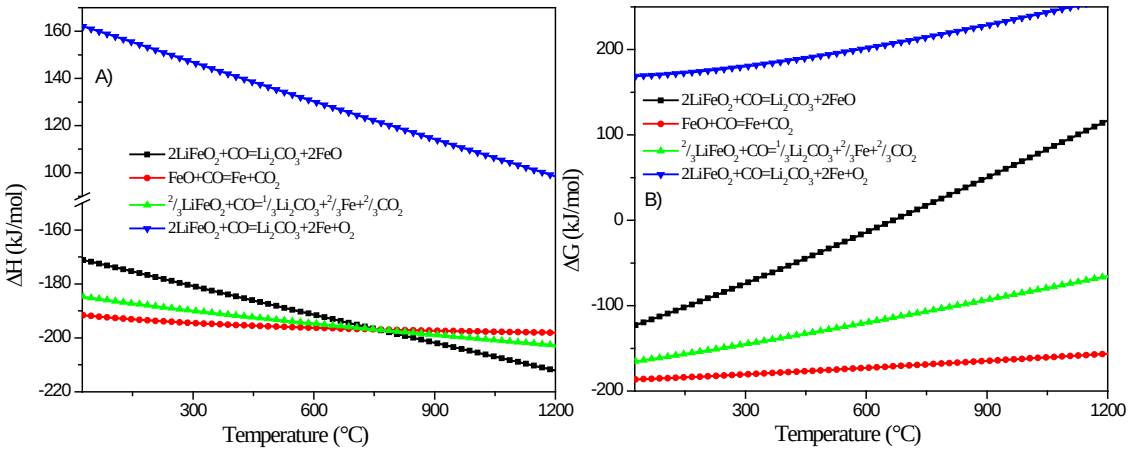
A)
B)
ΔH (kJ/mol)
ΔG (kJ/mol)
Temperature (°C)
Temperature (°C)
2LiFeO2+CO=Li2CO3+2FeO
FeO+CO=Fe+CO2
2/3LiFeO2+CO=1/3Li2CO3+2/3Fe+2/3CO2
2LiFeO2+CO=Li2CO3+2Fe+O2

Graphical Abstract